Short-pulse radiation by a sequentially excited semi-infinite periodic planar array of dipoles

Filippo Capolino[1]

Department of Electric and Computer Engineering, University of Houston, Houston, Texas, USA

Leopold B. Felsen[2]

Department of Aerospace and Mechanical Engineering, Boston University, Boston, Massachusetts, USA

Received 7 December 2001; revised 11 December 2002; accepted 19 February 2003; published 23 April 2003.

[1] This paper deals with the fourth in a sequence of canonical problems aimed toward an understanding of the time domain (TD) behavior of wideband-excited sequentially pulsed planar periodic finite arrays of dipoles, which play an important role in a variety of practical applications. The present investigation of sequentially pulsed semi-infinite planar dipole arrays extends our previous studies of sequentially pulsed infinite and semi-infinite line dipole arrays and of infinite planar dipole arrays. The discrete element-by-element radiations are converted collectively to radiations from a series of Floquet wave (FW)-modulated truncated smooth equivalent aperture distributions, and to corresponding FW-modulated edge diffraction. After a summary of necessary results from the earlier studies, emphasis is placed on the new truncation-induced TD results and interpretations, which are extracted via phenomenology-matched high-frequency asymptotics from rigorous frequency and time domain formulations parameterized in terms of the dispersive FW instantaneous frequencies and wave numbers. As in our previous studies, the outcome is a numerically efficient, physically incisive algorithm whose accuracy is verified preliminarily by application to a pulsed planar strip array of dipoles. *INDEX TERMS:* 0604 Electromagnetics: Antenna arrays; 0684 Electromagnetics: Transient and time domain; 0669 Electromagnetics: Scattering and diffraction; *KEYWORDS:* arrays, diffraction, floquet waves, periodic structures, time domain, transients

Citation: Capolino, F., and L. B. Felsen, Short-pulse radiation by a sequentially excited semi-infinite periodic planar array of dipoles, *Radio Sci.*, *38*(2), 8023, doi:10.1029/2001RS002588, 2003.

1. Introduction

[2] The prototype study of short-pulse radiation by a semi-infinite sequentially pulsed planar periodic array of dipoles (Figure 1) plays an important role in the efficient modeling of time-dependent radiation from, or scattering by, actual rectangular phased array antennas, frequency selective surfaces and related applications. Impulsive (delta function) excitations of the array elements, leading to the time domain (TD) Green's functions (GF), are analyzed here, as well as band-limited short-pulse excitations to model more realistic signals.

[3] Our approach is based on the exact equivalence between summation over the contributions from individual sequentially pulsed elements in an array and their collective treatment (via Poisson summation) in terms of infinite series of time domain (TD) Floquet waves (FW). We have already investigated the basic canonical TD-GFs for infinite [*Felsen and Capolino*, 2000] and truncated [*Capolino and Felsen*, 2002] periodic line arrays, and that for an infinite periodic planar array [*Capolino and Felsen*, 2003]. These cases have been parameterized, respectively, in terms of nontruncated or truncated conical TD-FWs [*Felsen and Capolino*, 2000; *Capolino and Felsen*, 2002], truncation-induced TD FW-modulated tip diffractions [*Capolino and Felsen*, 2002], and nontruncated planar TD-FWs [*Capolino and Felsen*, 2003], which furnish understanding of the corresponding FW

[1]Now at Department of Information Engineering, University of Siena, Siena, Italy.

[2]Also at Also at Polytechnic University, Brooklyn, New York, USA.

0048-6604/03/2001RS002588

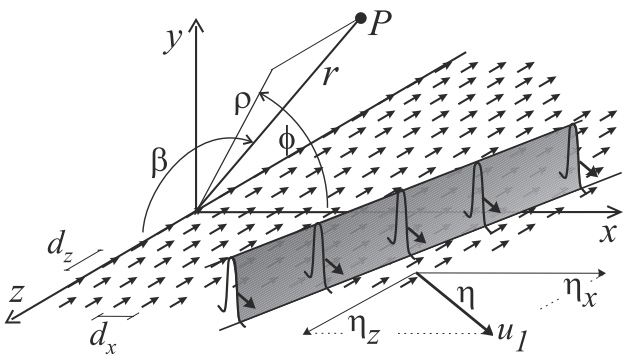

Figure 1. Physical configuration and coordinates for a planar periodic semi-infinite array of sequentially pulsed dipoles which excite a wavefront progressing along the u_1 coordinate on the array. ηk (with $\eta = (\eta_x^2 + \eta_z^2)^{1/2}$), phase gradient of the excitation along the direction u_1; $v_{u1}^{(p)} = c/\eta$, phase speed along u_1; $k = \omega/c$, c = ambient wave speed.

critical parameters and phenomenologies pertaining to time domain analysis of spatial periodicity. The present contribution extends the investigation of *Capolino and Felsen* [2003] to a semi-infinite periodic sequentially pulsed planar array, which introduces new truncation-induced TD phenomena.

[4] We proceed by accessing the time domain through asymptotic inversion of the frequency domain (FD) semi-infinite array results of *Capolino et al.* [2000b, 2000c], and obtain thereby the instantaneous frequencies that parameterize the behavior of the constituent TD-FWs. The problem is formulated in section 2. Section 3 contains a summary of the relevant FD results from *Capolino et al.* [2000b], prepared so as to facilitate the inversion to the TD, which is carried out in sections 4 and 5. Section 4 summarizes the TD-FW behavior for the infinite planar array investigated by *Capolino and Felsen* [2003] because these FWs play an essential role in building up the behavior for the semi-infinite case. Here emphasis is on the distinction between the non-dispersive lowest-order, and the dispersive higher-order TD-FWs. The TD-FW behavior for the semi-infinite array is developed in section 5, using the infinite array results in section 4 to parameterize and interpret truncation-induced phenomena affecting the bulk TD-FWs as well as giving rise to TD-FW-modulated diffractions from the array edge. Explaining these new TD results in section 5 in terms of band-limited (BL) problem-matched asymptotics implemented on the inversion integral (4) from the FD constitutes the main contribution in this paper. Preliminary numerical examples of radiation from a two-edged strip array with pulsed band-limited excitation in section 6 demonstrate the accuracy of the TD-FW algorithm and illustrate the rapid convergence of the (TD-FW)-based field representation since only a few terms are required for describing the off-surface field radiated by the truncated planar array. Conclusions are presented in section 7. Refinement and future calibration of these preliminary results through a systematic series of numerical experiments over broad ranges of parameters is reserved for a future publication.

2. Statement of the Problem

[5] The geometry of the array of parallel sequentially excited pulsed electric current dipole elements, oriented along the arbitrary vector direction $\mathbf{J}_0$ and radiating into free space, is shown in Figure 1. The array is infinite in the z direction and truncated in the x direction. Both cartesian and cylindrical reference coordinate systems with their z-axes along the array edge are introduced such that the array occupies the region $x > 0$, $y = 0$. The interelement period is d_x and d_z along the x and z directions, respectively. The $\mathbf{E}$ field component is simply related to the $\mathbf{J}_0$-directed magnetic scalar potential A which shall be used throughout. A caret ^ tags time-dependent quantities throughout and bold face symbols define vector quantities. With primed coordinates identifying generic source locations, any particular location is indexed by $(x', z') \equiv (nd_x, md_z)$, and the corresponding transient current excitations are denoted by $\hat{j}(nd_x, md_z, t)$, with the frequency (ω) and time (t) domains related via the Fourier transform pair

$$A(\omega) = \int_{-\infty}^{\infty} \hat{A}(t) e^{-j\omega t} dt, \quad \hat{A}(t) = \frac{1}{2\pi} \int_{-\infty}^{\infty} A(\omega) e^{j\omega t} d\omega. \tag{1}$$

The phased array FD and TD dipole currents $J(\omega)$ and $\hat{J}(t)$, respectively, are given by

$$\left.\begin{matrix} J(\omega) \\ \hat{J}(t) \end{matrix}\right\} = \sum_{m=-\infty}^{\infty} \sum_{n=0}^{\infty} \delta(x' - nd_x)\delta(z' - md_z) \cdot \left\{ \begin{matrix} e^{-jk(\eta_x x' + \eta_z z')} \\ \delta(t - (\eta_x x' + \eta_z z')/c) \end{matrix} \right\}, \tag{2}$$

where $k = \omega/c$ denotes the ambient wave number and c denotes the ambient wave speed. In the m, n-dependent element current amplitudes in the last factor in (2), $\omega\eta_x/c$ and $\omega\eta_z/c$ in the FD portion account for an assumed (linear) phase difference between adjacent elements in the x and z directions, respectively, with η_x/c and η_z/c as the interelement phase gradients normalized with respect to ω. The TD portion identifies sequentially pulsed dipole elements, with the element at $(x', z') = (nd_x, md_z)$ turned on at time $t_{mn} = (\eta_x nd_x + \eta_z md_z)/c$. The important

nondimensional single parameter, which is tied to the rotated coordinate system defined by u_1 (see Figure 1),

$$\eta = \sqrt{\eta_x^2 + \eta_z^2} = c\gamma_{u_1} = c/v_{u_1}^{(p)}, \tag{3}$$

combines both phasings η_x and η_z. In (3), $\gamma_{u1} = \eta/c = 1/v_{u1}^{(p)}$ is the normalized (with respect to ω) phase gradient along u_1, and $v_{u1}^{(p)} = c/\eta$ is the corresponding impressed phase speed. The TD cutoff condition $\eta = 1$ ($v_{u1}^{(p)} = c$) separates two distinct wave dynamics. For $\eta < 1$ the excitation phase speed $v_{u1}^{(p)} = c/\eta$ along u_1 is larger than the ambient wave speed c, and the projected phase speeds c/η_x and c/η_z along directions x and z are greater than c. Conversely, for $\eta > 1$, the excitation phase speed $v_{u1}^{(p)} = c/\eta$ of the array along u_1 is slower than c and will not be considered in this paper [see *Felsen and Capolino*, 2000; *Capolino and Felsen*, 2003] for some details about the more intricate but practically less important $\eta > 1$ case).

[6] Let the total (m, n)-summed frequency domain field at $\mathbf{r} \equiv (x, y, z)$, due to an array whose individual elements are excited by unit amplitude harmonic currents with phasing $\exp[-jk(\eta_x n d_x + \eta_z n d_z)]$ be represented by $A^{tot}(\mathbf{r}, \omega)$. The total time-dependent electric field excited by a band-limited (BL) signal is then given by

$$\hat{A}^{tot,BL}(\mathbf{r}, t) = \frac{1}{2\pi}\int_{-\infty}^{\infty} A^{tot}(\mathbf{r}, \omega) G(\omega) e^{j\omega t} d\omega, \tag{4}$$

in which $G(\omega)$ is the weight assigned to each frequency component. In our applications (see section 6), the pulse spectrum $G(\omega)$ is bounded away from $\omega = 0$ in such a manner as to render the high-frequency asymptotic expressions for $A^{tot}(\mathbf{r}, \omega)$ by *Capolino et al.* [2000b] valid over the entire bandwidth. Therefore the integral in (4) has portions that can be regarded as amplitude functions which vary slowly with frequency and as phase functions which oscillate rapidly, denoted by $F(\omega)$ and $\hat{\psi}(\omega)$, respectively, in (16), (32), and (36). This establishes the prerequisites for asymptotic evaluation in the ω domain. Since the composite phase function in (4) depends on space, time, and frequency, the asymptotic TD fields are parameterized by space-time-dependent saddle point frequencies found explicitly in the following sections.

3. Frequency-Domain Radiated FW Field: Preparation for TD Inversion

[7] It may be recalled that by Poisson summation, the sum of discretized element-by-element excitations in (2) can be converted into a sum of FW-modulated smoothly continuous equivalent source distributions covering the infinite (or semi-infinite) array aperture [see *Capolino et al.*, 2000b]. For convenience, we summarize below the relevant results of the FD-FW asymptotics for the magnetic vector potential, including FW-modulated diffracted fields, that were presented by [*Capolino et al.*, 2000b, Equations (14)–(16)] for the electric field. Also, we exhibit explicitly the ω dependences in anticipation of the TD inversion from the FD. Without loss of generality, due to symmetry, we restrict our analysis to the upper half-space $y > 0$. The radiated field (with a suppressed time dependence $\exp(j\omega t)$) is expressed as

$$A^{tot}(\mathbf{r}, \omega) = \sum_{p,q=-\infty}^{\infty} A_{pq}^{FW}(\mathbf{r}, \omega) U\left(\phi_{pq}^{SB} - \phi\right) + \sum_{q=-\infty}^{\infty} A_q^d(\mathbf{r}, \omega), \tag{5}$$

which contains infinite series of (pq)-indexed FW contributions A_{pq}^{FW} ($\mathbf{r}$, ω), and q-indexed diffracted fields $A_q^d(\mathbf{r}, \omega)$ arising from the edge of the array. The pqth FW in (5) is given by

$$A_{pq}^{FW}(\mathbf{r}, \omega) = \frac{e^{-j\left(k_{xp}x + k_{ypq}y + k_{zq}z\right)}}{2jd_x d_z k_{ypq}}, \tag{6}$$

and $U(\alpha) = 1$ or 0 for $\alpha > 0$ or $\alpha < 0$, respectively. The spectral wave numbers

$$k_{xp} = \eta_x \frac{\omega}{c} + \alpha_p, \qquad \alpha_p = \frac{2\pi p}{d_x}, \quad p = 0, \pm 1, \pm 2, \ldots \tag{7}$$

and

$$k_{zq} = \eta_z \frac{\omega}{c} + \alpha_q, \qquad \alpha_q = \frac{2\pi q}{d_z}, \quad q = 0, \pm 1, \pm 2, \ldots \tag{8}$$

represent the FW propagation coefficients (wave numbers) along x and z, respectively. Furthermore,

$$k_{ypq} = \sqrt{k^2 - k_{xp}^2 - k_{zq}^2}, \tag{9}$$

with the branch chosen to render $\Im m(k_{ypq}) \le 0$ on the top Riemann sheet; furthermore, $\Re e(k_{ypq}) \ge 0$ or $\Re e(k_{ypq}) \le 0$ for $\omega > 0$ or < 0, respectively, consistent with the radiation condition at $y = \infty$ for positive or negative frequencies. In (6), $k_{xp}^2 + k_{zq}^2 < k^2$ characterizes propagating FW while $k_{xp}^2 + k_{zq}^2 > k^2$ characterizes evanescent FWs. It is worth noting that the FW representation in (6) is the same as that for the infinite array, except for the Heaviside unit step function U in (5) that confines the domain of existence of the FWs to the region $\phi < \phi_{pq}^{SB}$ [see *Capolino et al.*, 2000c, Figures 1 and 2]. The angle ϕ_{pq}^{SB} denotes the shadow boundary (SB) of the pqth FW and, for propagating FWs, is given by *Capolino et al.* [2000b, equation (24)]:

$$\phi_{pq}^{SB} = \phi_{pq} = \cos^{-1}\left(\frac{k_{xp}}{k_{\rho q}}\right), \tag{10}$$

which also specifies the direction of the azimuthal component (in the (x, y) plane) of the pqth FW vector. In (10),

$$k_{\rho q} = \sqrt{k^2 - k_{zq}^2} \tag{11}$$

specifies the amplitude of the azimuthal (transverse-to-z) component of the pqth FW wave vector (see also the phase factor in (12)). As in (9), the branch is chosen to render $\Im m(k_{\rho q}) \leq 0$ on the top Riemann sheet, while $\Re e(k_{\rho q}) \geq 0$ or $\Re e(k_{\rho q}) \leq 0$ for $\omega > 0$ or < 0, respectively. The asymptotic evaluation of the qth diffracted FW field in (5), carried out by [*Capolino et al.* [2000b, section III-B], leads to

$$A_q^d(\mathbf{r}, \omega) \sim \frac{e^{-j\left(k_{\rho q}\rho + k_{zq} z\right)}}{2 d_z \sqrt{2\pi j k_{\rho q}\rho}} \cdot \left(\bar{B}_q(\omega) + \sum_{p=-P}^{P} \frac{F\left(\delta_{pq}^2\right) - 1}{j d_x k_{\rho q}\left(\cos\phi_{pq} - \cos\phi\right)}, \right) \tag{12}$$

in which $\bar{B}_q(\omega) = \frac{1}{2} + (j/d_x)\Sigma_{p=-\infty}^{\infty} [k_{\rho q}(\omega) \cos\phi - \eta_x\omega/c - \alpha_p]^{-1} = [1 - e^{jd_x[k_{\rho q}(\omega)\cos\phi - \eta_x\omega/c]}]^{-1}$, and F is the transition function of the Uniform Theory of Diffraction (UTD) [*Kouyoumjian and Pathak*, 1974],

$$F(x) = 2j\sqrt{x} e^{jx} \int_{\sqrt{x}}^{\infty} e^{-jt^2} dt, \quad \text{with } -\frac{3\pi}{2} < arg(x) \leq \frac{\pi}{2}, \tag{13}$$

whose arguments in (12) are given by

$$\delta_{pq}(\omega) = \sqrt{2 k_{\rho q}(\omega)\rho} \sin\left(\frac{\phi - \phi_{pq}(\omega)}{2}\right). \tag{14}$$

In (12), P denotes the number of poles extracted in the Van der Waerden procedure [see *Capolino et al.*, 2000b, equation (25)]. Owing to the exponential attenuation of the evanescent Floquet waves along y, the convergence of the (p, q) sum of FWs is very rapid away from the array plane. Furthermore, owing to the exponential decay along ρ of the evanescent diffracted FWs, the convergence of the q-sum of diffracted FWs is rapid away from the edge. Thus, in practice, only a few terms have to be retained in (5) to provide excellent approximations of the FD radiated field [see *Capolino et al.*, 2000c, section II-B].

4. Time Domain Floquet Waves for the Infinite Array

[8] Here we select from *Capolino and Felsen* [2003] those TD-FW$_{pq}$ results which bear directly on the truncation studies in section 5. Thus, for the present, we shall ignore the truncation SBs represented by the step function U in (5).

4.1. Nondispersive TD-FW$_{00}$

[9] The case $p = q = 0$ is nondispersive. This implies that the wave numbers in (7), (8), and (9) reduce for the $p = q = 0$ case to $k_{x,0} = \omega\eta_x/c$, $k_{z,0} = \omega\eta_z/c$, $k_{y,00} = \omega(1 - \eta^2)^{1/2}/c$; i.e., they are all linearly dependent on ω and therefore not amenable to saddle point evaluation. Inversion from the FD through the second relation in (1) with use of $A_{00}^{FW}(\mathbf{r}, \omega)$ from (6) yields the closed form (we only treat radiating FWs, for which $\eta < 1$, throughout this paper)

$$\hat{A}_{00}^{FW}(\mathbf{r}, t) = \frac{cU(t - t_0)}{2 d_x d_z \sqrt{1 - \eta^2}}, \tag{15}$$

with $t_0 = (\eta_x x + \eta_z z + \sqrt{1 - \eta^2} y)/c$ as has also been demonstrated after *Capolino and Felsen* [2003, equation (29)]. The TD-FW$_{00}$ is a planar step pulse turned on at time $t = t_0$.

4.2. Dispersive TD-FW$_{pq}$, With $p \neq 0$ or $q \neq 0$

[10] For $p \neq 0$ or $q \neq 0$, the TD-FW$_{pq}$ inversion integral becomes

$$\hat{A}_{pq}^{FW}(\mathbf{r}, t) = \int_{-\infty}^{\infty} F^{FW}(\omega) e^{-j\hat{\psi}(\omega)} d\omega, \tag{16}$$

in which $F^{FW}(\omega) = (4\pi j d_x d_z k_{ypq})^{-1}$, from (6), is considered slowly varying as a function of the radian frequency ω. The exponential term with

$$\hat{\psi}(\omega) = k_{xp} x + k_{zq} z + k_{ypq} y - \omega t, \tag{17}$$

in which k_{xp}, k_{zq}, and k_{ypq} are functions of ω as stated in (7), (8), and (9), is rapidly oscillatory. For these dispersive FWs with $p \neq 0$ or $q \neq 0$, the dominant contributions to the integral in (16) arise from the stationary (saddle) points $\omega_{pq,i}$ of $\hat{\psi}$ (ω) which satisfy $(d/d\omega)\, \hat{\psi}|_{\omega_{pq},i} = 0$. For p or $q \neq 0$, the real $\omega_{pq,i}$ solutions are found to be [see *Capolino and Felsen*, 2003, equation (44)],

$$\omega_{pq,i}(\mathbf{r}, t) = \bar{\omega}_{pq} + (-1)^i \tilde{\omega}_{pq} \frac{\tau}{\sqrt{\tau^2 - \tau_0^2}}, i = 1, 2, \tau > \tau_0, \tag{18}$$

with $\bar{\omega}_{pq} = \frac{c}{1 - \eta^2}(\eta_x\alpha_p + \eta_z\alpha_q)$, $\tilde{\omega}_{pq} = \frac{c}{1 - \eta^2}[(\eta_x\alpha_p + \eta_z\alpha_q)^2 + (\alpha_p^2 + \alpha_q^2)(1 - \eta^2)]^{1/2}$, and

$$\tau = t - (\eta_x x + \eta_z z)/c \tag{19}$$

$$\tau_0 = t_0 - (\eta_x x + \eta_z z)/c = \sqrt{1 - \eta^2} y/c. \tag{20}$$

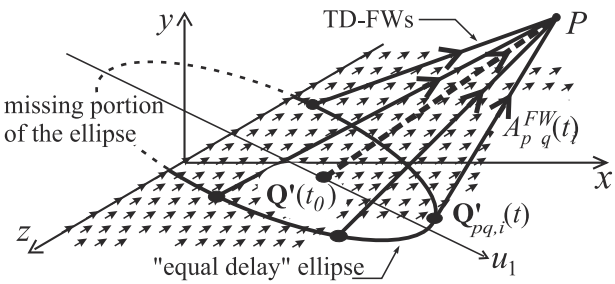

Figure 2. Propagating TD-FW phenomenology, based on radiation from the FW-modulated equivalent smoothly continuous source distribution on the infinite or semi-infinite array "aperture." u_1 points in the direction $\mathbf{u}_1 \equiv (\eta_x, 0, \eta_z)$ of the advancing excitation wavefront on the array (see Figure 1).

Evaluation of the pqth TD-FW integral in (16) via the standard asymptotic formula [*Felsen and Marcuvitz*, 1993, pp. 382]

$$\hat{A}^{FW}_{pq}(\mathbf{r},t) \sim \sum_{i=1}^{2} \hat{A}^{FW}_{pq,i} \tag{21}$$

$$\hat{A}^{FW}_{pq,i} \sim F^{FW}\left(\omega_{pq,i}\right) \frac{\sqrt{2\pi} e^{-j\hat{\psi}\left(\omega_{pq,i}(t)\right)}}{\sqrt{j(d^2/d\omega^2)\hat{\psi}|_{\omega_{pq,i}}}} U(\tau-\tau_0) \tag{22}$$

yields explicitly,

$$\hat{A}^{FW}_{pq,i}(\mathbf{r},t) \sim \frac{c e^{-j\left(\alpha_p x+\alpha_q z\right)} e^{-j(-i)^i \pi/4}}{d_x d_y \sqrt{2\pi(1-\eta^2)}} \cdot \frac{e^{j\left(\bar{\omega}_{pq}\tau+(-1)^i \bar{\omega}_{pq}\sqrt{\tau^2-\tau_0^2}\right)}}{\sqrt{\tilde{\omega}_{pq}}\left(\tau^2-\tau_0^2\right)^{1/4}} U(\tau-\tau_0). \tag{23}$$

The unit step function $U(\tau-\tau_0)$ arises because real saddle point frequencies $\omega_{pq,i}$ are restricted to $\tau > \tau_0$ ($t > t_0$). The range of validity of the FD-inverted asymptotic TD-FW in (23) is inferred from the analytic nondimensional estimator from *Capolino and Felsen* [2003, equation (55)] and plotted by *Capolino and Felsen* [2003, Figure 9]. Furthermore, (23) is the asymptotic version of the exact TD-FW evaluated by *Capolino and Felsen* [2003, equation (27)], and all interpretations relating to it apply here as well. The dispersive TD-FW$_{pq}$ has the same turn on time t_0 as the nondispersive TD-FW$_{00}$.

[11] As shown by *Capolino and Felsen* [2003, equation (57)], the observation point $\mathbf{r} \equiv (x, y, z)$, together with the local instantaneous frequencies and their corresponding local instantaneous wave numbers in (7)–(9), $k_{xp}(\omega_{pq,i}(t))$, $k_{zq}(\omega_{pq,i}(t))$ and $k_{ypq}(\omega_{pq,i}(t))$, define localized points of "emergence" $\mathbf{Q}'_{pq,i}(t) = [x'_{pq,i}(t), z'_{pq,i}(t)] \equiv [x - y k_{xp}(\omega_{pq,i}(t))/k_{ypq}(\omega_{pq,i}(t)), z - y k_{zq}(\omega_{pq,i}(t))/k_{ypq}(\omega_{pq,i}(t))]$ from the FW-modulated equivalent continuous source distribution on the array plane (a few such points are shown in Figure 2). Thus the first signal arrival at the observation point $\mathbf{r} \equiv (x, y, z)$ originates at the earlier point $\mathbf{Q}'(t_0) = [x'(t_0), z'(t_0)] \equiv [x - y\eta_x(1-\eta^2)^{-1/2}, z - y\eta_z(1-\eta^2)^{-1/2}]$. Successively, for $t > t_0$, these $\mathbf{Q}'_{pq,i}(t)$ points all lie on the t-instantaneous "equal delay" ellipse defined by *Capolino and Felsen* [2003, equation (58)] and schematized in Figure 2. At each time t, all TD-FW$_{pq}$ propagate toward the observer along a t-dependent cone with the same group velocity c. For the semi-infinite array, the observer is reached only by those TD-FWs that were launched from points with $x'_{pq,i}(t) > 0$ on the actual array, i.e., when the launch points lie on the solid part of the ellipse (Figure 2). The corresponding phenomenology is schematized in sections 5.2 and 5.3.

5. Time Domain Floquet Waves for the Semi-Infinite Array: Truncation of TD-FWs and Truncation-Induced TD Diffraction

[12] "Bulk" TD-FWs for the truncated planar array behave in the same way as those for the infinite planar array except for the presence of shadow boundaries that delimit their region of existence. Additionally, a diffracted field arising from the edge truncation at $x = 0$ exhibits FW-modulated q-dependent dispersive ($q \neq 0$) and nondispersive ($q = 0$) behavior. Inversion from the FD total radiated field in (5) leads to

$$\hat{A}^{tot}(\mathbf{r},t) = \sum_{q=-\infty}^{\infty} \frac{1}{2\pi} \int_{-\infty}^{\infty} \left[\sum_{p=-\infty}^{\infty} A^{FW}_{pq}(\mathbf{r},\omega) \cdot U\left(\phi^{SB}_{pq}(\omega) - \phi\right) + A^{d}_{q}(\mathbf{r},\omega) \right] e^{j\omega t} d\omega. \tag{24}$$

Three distinct cases are distinguished, based on the p,q-dependent FD dispersion relations for FWs and diffracted fields which are summarized in Table 1 and analyzed in sections 5.1, 5.2, and 5.3, respectively. In Table 1, the azimuthal angle $\phi^{SB}_{pq}(\omega)$ defined in (10) denotes the SB and direction of propagation of the pqth propagating FW, and $k_{\rho q}(\omega)$ is the radial wave number, in (11), of the q-th diffracted field. We focus here only on propagating FWs since all the impulsively excited FD-FW$_{pq}$ in (6) are propagating when evaluated at their instantaneous frequencies $\omega_{pq,i}(t)$ in (18), as shown in (23).

Table 1. Dispersive Behavior of the pqth FW and Associated Diffracted Fields

	FD-FW Direction of Propagation	FD-Diffracted Field Radial Wave Number
$q = p = 0$	$\cos\phi_{00}(\omega) = \eta_x/\sqrt{1-\eta_z^2}$ nondispersive FW	$k_{\rho 0}(\omega) = (\omega/c)\sqrt{1-\eta_z^2}$ nondispersive diffracted field
$q = 0$ and $p \neq 0$	$\cos\phi_{p0} = (\omega\eta_x + \alpha_p)/k_{\rho 0}(\omega)$ dispersive FW	$k_{\rho 0}(\omega) = (\omega/c)\sqrt{1-\eta_z^2}$ nondispersive diffracted field
$q \neq 0$	$\cos\phi_{pq} = (\omega\eta_x + \alpha_p)/k_{\rho q}(\omega)$ dispersive FW	$k_{\rho q}(\omega) = \sqrt{(\omega/c)^2 - (\omega\eta_z/c + \alpha_q)^2}$ dispersive diffracted field

[13] For $p = q = 0$, the SB angle and direction of propagation of FD-FW$_{00}$ do not depend on ω, and the radial wave number is linearly dependent on ω. This case is therefore nondispersive. For $q = 0$ and $p \neq 0$, FWs are dispersive since the SB angle and direction of propagation vary with ω as shown in Table 1. The $q = 0$ diffracted field is nondispersive because its radial wave number $k_{\rho 0}(\omega)$ still depends linearly on ω (however, this field becomes "weakly dispersive" in the transition region surrounding the SB so as to match the phase speed there of the dispersive FD-FW$_{p0}$). For $q \neq 0$ (and arbitrary p), both the FW and diffracted fields are dispersive since their directions of propagation vary with ω (the FW and diffracted wave numbers depend nonlinearly on ω).

[14] For frequency-dependent SBs (i.e., $q \neq 0$ and/or $p \neq 0$) and a fixed observer at ϕ, there is a particular frequency ω_{pq}^{SB} such that

$$\phi_{pq}^{SB}\left(\omega_{pq}^{SB}\right) = \phi, \tag{25}$$

which is determined by squaring and rearranging the expression $\cos\phi_{pq}^{SB}(\omega) = \cos\phi$ (see (10)). One obtains $\frac{\omega^2}{c^2}[(1-\eta_z^2)\cos^2\phi - \eta_x^2] - 2\frac{\omega}{c}(\eta_x\alpha_p + \eta_z\alpha_q\cos^2\phi) - (\alpha_p^2 + \alpha_q^2\cos^2\phi) = 0$, with solutions

$$\omega_{pq}^{SB} = c\frac{\left(\eta_x\alpha_p + \eta_z\alpha_q\cos^2\phi\right) \pm \cos\phi\sqrt{\alpha_p^2 + \alpha_q^2\cos^2\phi - \left(\eta_x\alpha_q - \eta_z\alpha_p\right)^2}}{\left(1-\eta_z^2\right)\cos^2\phi - \eta_x^2}. \tag{26}$$

The illuminated region constraint $\phi < \phi_{pq}^{SB}(\omega)$ on the FD-FWs in (24) implies that for p and/or $q \neq 0$, the FD-FWs and diffracted fields are individually ω-discontinuous at $\omega = \omega_{pq}^{SB}$, although their sum $A_{pq}^{FW}(\mathbf{r}, \omega)U(\phi_{pq}^{SB}(\omega) - \phi) + A_q^d(\mathbf{r}, \omega)$ is continuous there. The ω_{pq}^{SB} radian frequencies will play an important role in the discontinuity-induced compensation mechanisms discussed in section 5.3.

[15] The three FW$_{pq}$ dispersion regimes in Table 1 parameterize subsequent high-frequency asymptotics for the FD-FW and diffracted fields in (24) away from the transition regions near the shadow boundaries where $\omega \approx \omega_{pq}^{SB}$. Nonuniform asymptotics leads to the FW-modulated ray optical interpretation of the relevant wave phenomenology. Near the SB$_{pq}$ one needs to employ uniform asymptotics for the diffracted fields, given in (12). Far from SBs, i.e., for ω substantially different from ω_{pq}^{SB}, the temporal dispersion of the diffracted field (12) is dominated by $\exp[-jk_{\rho q}(\omega)\rho]$, as noted in Table 1, since $\delta_{pq}^2(\omega) \gg 1$ and thus $F[\delta_{pq}^2(\omega)] \approx 1$. However, in the pqth transition region, the diffracted field assumes a transitional behavior so as to match the phase speed of the FD-FW$_{pq}$ at the SB$_{pq}$, thereby changing its dispersion properties. We recall that the expression for the qth diffracted field in (12) compensates for the SB-discontinuity of all propagating pqth FD-FWs that have been regularized via the Van der Waerden procedure (i.e., those with extracted poles in $-P \leq p \leq P$). Approaching the SB$_{pq}$, $\delta_{pq}^2(\omega) \approx 0$, whence $F(\delta_{pq}^2 \approx 0) \approx \sqrt{\pi j\delta_{pq}^2}\exp(j\delta_{pq}^2) \approx 0$. This locally dispersive transitional behavior permits the qth FD diffracted field to compensate for the discontinuity of the pqth FD-FW at the SB$_{pq}$, as explained by *Capolino et al.* [2000c, section III-A]. One finds that $A_q^d(\mathbf{r},\omega) \approx \frac{1}{2}sgn[\phi - \phi_{pq}^{SB}(\omega)]A_{pq}^{FW}(\mathbf{r}, \omega) \propto \exp[-j(k_{xp}x + k_{ypq}y + k_{zq}z)]$, which matches the dispersive exponent of the FD-FW. This transitional phenomenology pertains to the cases treated in sections 5.2 and 5.3.

5.1. Nondispersive TD Diffracted Field $q = 0$ and $p = 0$

[16] As shown in Table 1, the SB ϕ_{00}^{SB} is independent of ω and the Fourier inversion (24) is carried out separately for the two terms $A_{00}^{FW}(\mathbf{r}, \omega)U(\phi_{00}^{SB} - \phi)$ and $A_0^d(\mathbf{r}, \omega)$. Fourier inversion of $A_{00}^{FW}(\mathbf{r}, \omega)$ produces the TD-FW in (15). A few steps have to be carried out before the inversion of $A_0^d(\mathbf{r}, \omega)$. Referring to (12) we write (with explicit insertion of the ω-dependence), $\bar{B}_0(\omega) = \frac{1}{2} + (j/d_x)\sum_{p=-\infty}^{\infty}[\frac{\omega}{c}(1-\eta_z^2)^{1/2}(\cos\phi - \cos\phi_{00}) - \alpha_p]^{-1}$. We also decompose the "quasi nondispersive" $q = 0$ diffracted field in (12) into $A_0^d(\mathbf{r}, \omega) = A_{00}^d(\mathbf{r}, \omega) + \sum_{p\neq 0}A_{p0}^d(\mathbf{r}, \omega)$, with

$$A_{00}^d(\mathbf{r},\omega) = \frac{\sqrt{c}\,e^{-j\omega t_d}}{2d_z\sqrt{2\pi j\omega\sqrt{1-\eta_z^2}\rho}} \cdot \left[\frac{1}{2} + \frac{cF\left(\delta_{00}^2\right)}{jd_x\omega\sqrt{1-\eta_z^2}(\cos\phi_{00} - \cos\phi)}\right] \tag{27}$$

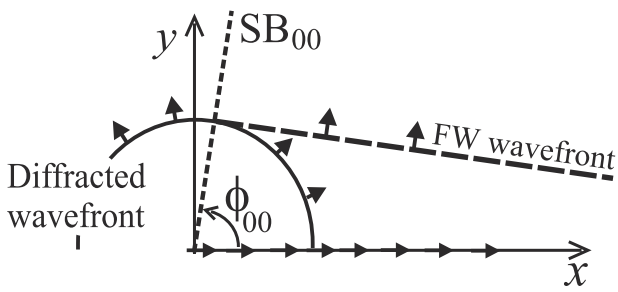

Figure 3. $p = q = 0$ TD-FW and diffracted wavefront phenomenologies in the transverse x-y plane. The planar TD-FW wavefront of $\hat{A}_{00}^{FW}$ and the conical diffracted field wavefront of $\hat{A}_0^d$ reach the observer at $t = t_0$ and $t = t_d \geq t_0$, respectively. Adding the TD-diffracted field to the truncated TD-FW restores continuity at the SB along and behind the wavefront.

arising from the 1/2 and $p = 0$ terms in $\bar{B}_0(\omega)$, and $\Sigma_{p\neq 0} A_{p0}^d$ taking into account all higher-order p-terms as shown later on in section 5.2. In (27), $t_d = (\sqrt{1-\eta_z^2}\rho + \eta_z z)/c$, $\delta_{00}^2 = 2\,\omega c^{-1}\sqrt{1-\eta_z^2}\rho \sin^2[(\phi - \phi_{00})/2] = \omega\,(t_d - t_0)$. The last identity is obtained using $\cos\phi = x/\rho$, $\cos\phi_{00} = \eta_x/\sqrt{1-\eta_z^2}$, observing that $2\rho \sin^2[(\phi - \phi_{00})/2] = \rho - \rho\cos(\phi - \phi_{00}) = (\rho\sqrt{1-\eta_z^2} - x\eta_x - y\sqrt{1-\eta^2})/\sqrt{1-\eta_z^2}$, and recalling (20). The Fourier inversion of (27) can be carried out in closed form via an exact transform based on the formula (see expression before (23) and (50) of *Capolino and Felsen* [2002] followed by a convolution),

$$\begin{aligned}\hat{I}(t) &= \frac{1}{2\pi}\int_{-\infty}^{\infty} \frac{F[\omega(t_d - t_0)]}{j\omega\sqrt{j\omega}} e^{j\omega(t-t_d)} d\omega \\ &= 2\frac{\sqrt{t_d - t_0}}{\sqrt{\pi}} \sin^{-1}\left(\frac{\sqrt{t-t_d}}{\sqrt{t-t_0}}\right) U(t-t_d),\end{aligned} \tag{28}$$

which leads to

$$\begin{aligned}\hat{A}_{00}^d(\mathbf{r},t) = &\frac{1}{2\pi d_z\sqrt{2\tau_d}} \\ &\cdot \left[\frac{1/2}{\sqrt{t-t_d}} + \frac{2c\sqrt{t_d - t_0}\sin^{-1}\left(\frac{\sqrt{t-t_d}}{\sqrt{t-t_0}}\right)}{d_x\sqrt{(1-\eta_z^2)}(\cos\phi_{00} - \cos\phi)}\right] \\ &\cdot U(t-t_d),\end{aligned} \tag{29}$$

with

$$\tau_d = t_d - \eta_z z/c = \sqrt{1-\eta_z^2}\rho/c. \tag{30}$$

Near the SB $\phi = \phi_{00}$ (where $t_d = t_0$) we have $\sqrt{t_d - t_0} = \sqrt{2\tau_d}\sin((\phi - \phi_{00})/2) \to 0$, which compensates for the discontinuity in the denominator of the second term in (29) (see Figure 3). The TD Fourier inversion of all the other p-terms (with $q = 0$) $A_{p0}^d(\mathbf{r}, \omega)$ is treated next.

5.2. "Weakly Dispersive" TD Diffracted Fields With $q = 0$ and $p \neq 0$

[17] To perform the asymptotic inversion of $A_{p0}^T \equiv A_{p0}^{FW}(\mathbf{r}, \omega)\, U[\phi_{p0}^{SB}(\omega) - \phi] + A_{p0}^d(\mathbf{r}, \omega)$ for $q = 0$ and $p \neq 0$, we treat FW portion as in section 4.2 and use an approximate form of the diffracted field valid when the space-time position of the observer is in the vicinity of the SB. The relevant expression for the FD diffracted field

$$A_{p0}^d(\mathbf{r},\omega) \sim \frac{e^{-j\left(k_{\rho 0}\rho + k_{z0}z\right)}}{2d_z\sqrt{2\pi j k_{\rho 0}\rho}} \frac{F\left[\delta_{p0}^2\right]}{j d_x k_{\rho 0}\left[\cos\phi_{p0} - \cos\phi\right]} \tag{31}$$

arises from the higher-order p-terms in $\bar{B}_0(\omega)$ (above (27)), combined with (12), in which $k_{\rho 0}(\omega)$, $k_{z0}(\omega)$, $\phi_{p0}(\omega)$ and $\delta_{p0}^2(\omega)$ are all functions of ω. The corresponding inverted TD-FW, valid away from and near the SB, is obtained as in section 4.2 for the infinite array, using the dominant instantaneous frequencies $\omega_{p0,i}(t)$ also in the shadow boundary truncation functions $U[\phi_{p0}(\omega_{p0,i}(t)) - \phi]$, $i = 1, 2$. A simple expression for the TD diffracted fields $\hat{A}_{p0}^d(\mathbf{r}, t)$ can be derived when the observer is close to the moving SB_{p0} where $\omega \approx \omega_{p0}^{SB}$. Therefore $\phi \approx \phi_{p0}(\omega)$ in (31). and the argument of the transition function F becomes $\delta_{p0}(\omega \approx \omega_{p0}^{SB}) \approx 0$ (see (14)), yielding $F \approx \sqrt{\pi j\delta_{p0}^2}\,\exp(j\delta_{p0}{}^2)$, as verified from the relations $F(\delta^2) = \pm\sqrt{\pi}e^{j\pi/4}\delta e^{j\delta^2} erfc(\pm e^{j\pi/4}\delta)$, $erfc(z) = (2/\sqrt{\pi})\int_z^\infty e^{-u^2}du$, with the upper/lower signs applying for $\Re e(e^{j\pi/4}\delta) \gtrless 0$ [*Capolino et al.*, 2000b; *Rojas*, 1987]. Noting that $-k_{\rho 0}(\omega)\rho + \delta_{p0}^2(\omega) = -[k_{xp}(\omega)x + k_{yp0}(\omega)y]$ (using (10)), the resulting inversion of $A_{p0}^T(\mathbf{r}, \omega)$ near the SB becomes

$$\hat{A}_{p0}^T(\mathbf{r},t) \sim \int_{-\infty}^{\infty} F^T(\omega) e^{-j\widehat{\psi(\omega)}} d\omega, \tag{32}$$

were $\hat{\psi}(\omega)$, defined in (17), takes into account the phase terms, and

$$\begin{aligned}F^T(\omega) = &\frac{U\left[\phi_{p0}^{SB}(\omega) - \phi\right]}{4\pi j d_x d_z k_{y,p0}} \\ &+ \frac{1}{4\pi j d_x d_z\sqrt{2k_{\rho 0}\rho}} \frac{\pm\delta_{p0} erfc\left(\pm e^{j\pi/4}\delta_{p0}\right)}{k_{\rho 0}\left[\cos\phi_{p0}^{SB} - \cos\phi\right]}\end{aligned} \tag{33}$$

is the slowly varying part of $A_{p0}^T(\mathbf{r}, \omega)$ near the SB.

[18] As in section 4.2, the dominant contributions to the integral in the high-frequency range arise from the stationary (saddle) points $\omega_{p0,i}(t)$ of $\hat{\psi}(\omega)$ given in (18).

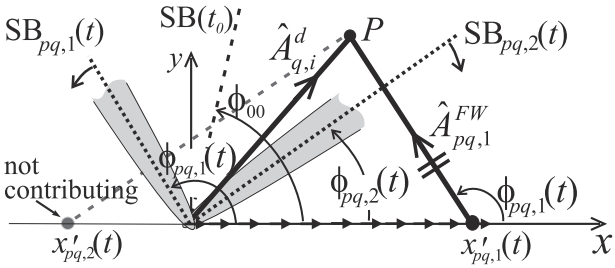

Figure 4. Moving shadow boundaries for dispersive FWs and moving transition regions (parabolas around SBs) for diffracted fields. At the instant t_0, the SBs of all FWs coincide with SB(t_0), i.e., $\phi_{pq,1}(t_0) = \phi_{pq,2}(t_0) = \phi_{00}$. At later instants $t > t_0$, they separate into $SB_{pq,i}(t)$, $i = 1$, 2, forming angles $\phi_{pq,i}(t) \equiv \phi_{pq}^{SB}(\omega_{pq,i}(t))$ with the x-axis, such that $\phi_{pq,1}(t) > \phi_{00} > \phi_{pq,2}(t)$. Observing that $k_{\rho q} = (k_{xp}^2 + k_{zq}^2)^{1/2}$ and thus $|\cos \phi_{pq,i}(t)| \leq 1$ (see (10)), implies that the angles $\phi_{pq,i}(t)$ are real for any p and any $t > t_0$ and that all the TD-FW_{pq} are propagating toward the observer. According to (43), the $FW_{pq,i}$ are confined to the right side of $SB_{pq,i}(t)$ for $i = 1$, 2, respectively. Recalling Figure 2, the observer is reached only by those FWs $\hat{A}_{pq,i}^{FW}$ that originate at points $x'_{pq,i}(t) = x - y \cot\phi_{pq,i}(t) > 0$. The FW-existence conditions $x'_{pq,i}(t) > 0$ or $\phi < \phi_{pq,i}(t)$ are equivalent, i.e., $U(\phi_{pq,i}(t) - \phi) \equiv U(x'_{pq,i}(t))$.

In (33), *erfc* is considered as an amplitude function as did *Capolino and Felsen* [2002], [*Carin and Felsen* [1993], and *Felsen and Carin* [1994] because over its effective range $\phi_{p0}(\omega) \approx \phi$ (in the proximity of the SB), its phase varies slowly. (Away from the SB, the phase varies rapidly; there, however, the FW field is not discontinuous and the diffracted field may either be neglected without appreciable loss of accuracy or evaluated by other techniques. Better approximations for the diffracted field away from the shadow boundaries are beyond the scope of the present investigation). The asymptotic evaluation of (32) is carried out via the formula in (21), with (33), and $(d^2/d\omega^2)\hat{\psi}|_{\omega p0,i} = y(1 - \eta^2)^2 c^{-4} \tilde{\omega}_{p0}^2 k_{yp0,i}^{-3}$. This leads to $\hat{A}_{p0,i}^{T}(\mathbf{r}, t) = \sum_{i=1}^{2} \hat{A}_{p0,i}^{T}$, with

$$\hat{A}_{p0,i}^{T}(\mathbf{r}, t) \sim \hat{A}_{p0,i}^{FW}(\mathbf{r}, t) U\left[\phi_{p0,i}(t) - \phi\right] + \hat{A}_{p0,i}^{d}(\mathbf{r}, t), \tag{34}$$

in which $\hat{A}_{p0,i}^{FW}(\mathbf{r}, t)$ is the same as in (23). The Heaviside function U terminates the TD-FW_{p0} domain of existence at the moving shadow boundary plane $\phi = \phi_{p0,i}(t) \equiv \phi_{p0}(\omega_{p0,i}(t))$ with $\cos\ \phi_{p0}(\omega_{p0,i}(t)) = k_{xp}(\omega_{p0,i}(t))/k_{\rho 0}(\omega_{p0,i}(t)) = [\eta_x + \alpha_p c/\omega_{p0,i}(t)]/\sqrt{1 - \eta_z^2}$. The diffracted field is

$$\hat{A}_{p0,i}^{d}(\mathbf{r}, t) \sim \frac{e^{j\omega_{p0,i}(t)\cdot\left(t - t^{d}\right)}}{2d_z\sqrt{2\pi j k_{\rho 0,i}(t)\rho}} \cdot \frac{F\left[\delta_{p0,i}^2(t)\right]}{jd_x k_{\rho 0,i}(t)\left(\cos\phi_{p0,i}(t) - \cos\phi\right)} \cdot \frac{e^{(-1)^i j\pi/4}\tau_0\sqrt{2\pi\tilde{\omega}_{p0}}}{\left(\tau^2 - \tau_0^2\right)^{3/4}} U(t - t_0), \tag{35}$$

where $\omega_{p0,i}(t)$, and therefore $\phi_{p0,i}(t)$, $k\rho_{0,i}(t) \equiv \sqrt{1 - \eta_z^2}\omega_{p0,i}(t)/c$ and $\delta_{p0,i}(t) \equiv \delta_{p0}(\omega_{p0,i}(t))$, are functions of t. We refer to Figure 4 and its caption for the moving SB behavior for $t \geq t_0$. At a time t, an arbitrarily located observer is always reached by the diffracted fields $\hat{A}_{p0,i}^{d}$, $i = 1,2$ but only by those truncated FWs $\hat{A}_{p0,i}^{FW}$ that originate at points $x'_{p0,i}(t) > 0$ and illuminate the observation point (see schematic in Figures 2 and 4).

5.3. Strongly Dispersive Diffracted Fields With $q \neq 0$

[19] Due to the dispersive behavior of the diffracted fields with $q \neq 0$, inversion into the TD is carried out via local instantaneous diffracted frequencies. As previously, "far" from the SB_{pq} (with arbitrary p), the diffracted field dispersion is dominated by $\exp[-j\ k_{\rho q}(\omega)\rho]$, (see (12) and Table 1). In that domain, where ω differs substantially from ω_{pq}^{SB}, the Fourier inversion (24) of the A_q^d ($\mathbf{r}$, ω) term in (12) yields

$$\hat{A}_q^d(\mathbf{r}, t) \sim \int_{-\infty}^{\infty} F^d(\omega) e^{-j\hat{\psi}^d(\omega)} d\omega, \quad q \neq 0, \tag{36}$$

where

$$\hat{\psi}^d(\omega) = k_{zq} z + k_{\rho q}\rho - \omega t, \tag{37}$$

with $k_{zq}(\omega)$ and $k_{\rho q}(\omega)$ given in (8) and (11), respectively, takes into account the phase terms, whereas $F^d(\omega) = D(\omega)/[4\pi\ d_z\sqrt{2\pi j k_{\rho q}(\omega)\rho}]$ is the slowly varying part of A_q^d ($\mathbf{r}$, ω), with $D(\omega)$ denoting the expression inside the brackets in (12). The dispersion relation in (37) coincides with that of the different but analogous canonical problem of *Felsen and Capolino* [2000]. For these dispersive diffracted fields, the dominant contributions to the integral in (36) arise from the real stationary (saddle) point solutions $\omega_{q,i}^d$ of $\hat{\psi}^d(\omega)$, which satisfy $(d/d\omega)\hat{\psi}^d|_{\omega_{q,i}^d} = 0$ [see *Felsen and Capolino*, 2000, Appendix A],

$$\omega_{q,i}^d(\mathbf{r}, t) = \frac{c}{1 - \eta_z^2}\left(\alpha_q\eta_z + \frac{(-1)^i|\alpha_q|\tau'}{\sqrt{\tau'^2 - \tau_d^2}}\right), \quad i = 1, 2, \qquad \tau' > \tau_d \tag{38}$$

with

$$\tau' = t - \eta_z z/c \tag{39}$$

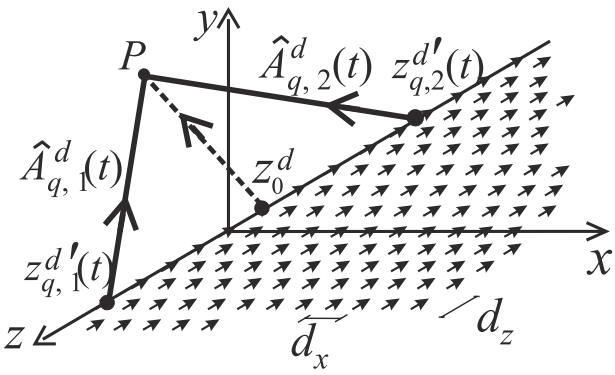

Figure 5. Edge-diffracted field phenomenology. At the turn-on time $t = t_d$, all diffracted fields $\hat{A}^d_{q,i}(t)$ arriving at the observation point P were generated at an earlier time point $z^d_{q,1'}(t_d) = z^d_{q,2'}(t_d) \equiv z^d_0$. For $t > t_d$, the two points $z^d_{q,1'}(t)$ and $z^d_{q,2'}(t)$ are the earlier points of emergence of all diffracted fields which arrive simultaneously.

and τ_d defined in (30). For each FW order q, the two real solutions $i = 1, 2$ yield the two field contributions shown in Figure 5. These diffracted field local instantaneous frequency solutions $\omega^d_{q,i}(\mathbf{r}, t)$ are the same as those of *Felsen and Capolino* [2000, equation (28)] and they match the order of the $\omega_{pq,i}(\mathbf{r}, t)$ solutions in (18) at a given point $\mathbf{r}$ and a given instant t in the causal domain $\tau' > \tau_d$ or $t > t_d = \eta_z z/c + \tau_d$. At turn-on $t = t_d$, $|\omega^d_{q,i}| \to \infty$ for all q (see Figure 6). The frequencies increase with FW mode index q, decrease with time t, and approach their cutoff value $\omega^d_{q,i}(t \to \infty) = \omega^{d,cutoff}_{q,i} = c(1 - \eta_z^2)^{-1}[\alpha_q\eta_z + (-1)^i |\alpha_q|]$, defined by $|k_{zq}(\omega)| = |k(\omega)|$ or, alternatively, by $k_{\rho q}(\omega) = 0$ (see (11)). The corresponding instantaneous wave numbers $k^d_{q,i}(t) \equiv k(\omega^d_{q,i}(\mathbf{r}, t))$, $k^d_{zq,i}(t) \equiv k_{zq}(\omega^d_{q,i}(\mathbf{r}, t))$, and $k^d_{\rho q,i}(t) \equiv k_{\rho q}(\omega^d_{q,i}(\mathbf{r}, t))$, obtained from (8) and (11), are all real for $t > t_d$, and the FD diffracted fields are all propagating when evaluated at $\omega^d_{q,i}(\mathbf{r}, t)$ since $|k^d_{q,i}(t)| > |k^d_{zq,i}(t)|$ [see *Felsen and Capolino*, 2000, section V-B]. The points of emergence $z^{d\prime}_{q,i}(t)$ located on the edge (see Figure 5) are defined by $z^{d\prime}_{q,i}(t) = z - \rho k^d_{zq,i}(t)/k^d_{\rho q,i}(t) = z - (1 - \eta_z)^{-1}[\eta_z\tau' + (-1)^i sgn(\alpha_q)\sqrt{\tau'^2 - \tau_d^2}]$ which depend only on the sign of q. The asymptotic evaluation of the integral (36) is carried out via the formula in (21)–(22) (adapted to the $\hat{A}^d_q$ format). From (17) and (38), one finds $\hat{\psi}^d(\omega^d_{q,i}(t)) = \alpha_q z^{d\prime}_{q,i}(t)$ and $(d^2/d\omega^2)\hat{\psi}^d|_{\omega^d_{q,i}} = -\rho\alpha_q{}^2/[c^2(k^d_{\rho q,i}(t))^3]$, which yields $\hat{A}^d_q(\mathbf{r}, t) = \Sigma_{i=1}^2 \hat{A}^d_{q,i}$, with

$$\hat{A}^d_{q,i}(\mathbf{r}, t) \sim \frac{e^{-j\alpha_q z^{d\prime}_{q,i}(t)} U(\tau' - \tau_d)}{4\pi d_z\sqrt{\tau'^2 - \tau_d^2}} D\left(\omega^d_{q,i}(t)\right), \qquad i = 1, 2, \tag{40}$$

where $D(\omega)$ is the expression inside the brackets in (12). The resulting expression in (40) is restricted to early observation times because it is based on the inversion of the high-frequency representation of the FD-FW on the right side of (24) and (36) [see *Felsen and Marcuvitz*, 1973]. TD-FW with $q \neq 0$ are evaluated via their local instantaneous frequencies $\omega_{pq,i}(t)$ in (18), as in section 4.2 when $\omega_{pq,i}(t)$ differs substantially from ω^{SB}_{pq}. The only addition is that the U function in (24) is also evaluated at the FW instantaneous frequency leading to $\Sigma_{i=1}^2 \hat{A}^{FW}_{pq,i}(\mathbf{r}, t)U[\phi_{pq,i}(t) - \phi]$, in which the TD-FW $\hat{A}^{FW}_{pq,i}(\mathbf{r}, t)$ is the same as in (23) and the moving shadow boundary $\phi_{pq,i}(t) \equiv \phi_{pq}(\omega_{pq,i}(t)$ with $\cos\phi_{pq}(\omega_{pq,i}(t)) = k_{xp}(\omega_{pq,i}(t))/k_{\rho q}(\omega_{pq,i}(t))$. We refer to Figure 4 and its caption for the moving SB behavior for $t \geq t_0$. We show hereafter that the condition "$\omega_{pq,i}(t)$ substantially different from ω^{SB}_{pq}" is equivalent to "$\omega^d_{q,i}(t)$ substantially different from ω^{SB}_{pq}."

[20] In the SB_{pq} transition region, where the local instantaneous frequencies $\omega^d_{q,i}(t)$ are close to ω^{SB}_{pq}, the simple asymptotics above cannot be applied because $F^d(\omega)$ in (36) is now rapidly oscillating for $\omega \approx \omega^{SB}_{pq}$, one has $\delta^2_{pq}(\omega) \approx 0$ and $F \approx \sqrt{\pi j\delta^2_{pq}}\exp(j\delta^2_{pq})$, which introduces the additional phase term $\exp(j\delta^2_{pq})$. Recalling (14) and that $\delta^2_{pq} = k_{\rho q}\rho[1 - \cos(\phi - \phi_{pq})] = k_{\rho q}\rho - k_{xp}x - k_{ypq}y$ (using (10)), one observes that

$$\psi^d(\omega) - \delta^2_{pq}(\omega) = \psi(\omega), \tag{41}$$

where $\psi(\omega)$ given in (17) represents the total phase (including $\exp(j\omega t)$) of $A^d_q(\mathbf{r}, \omega)$, for $\omega \approx \omega^{SB}_{pq}$. This

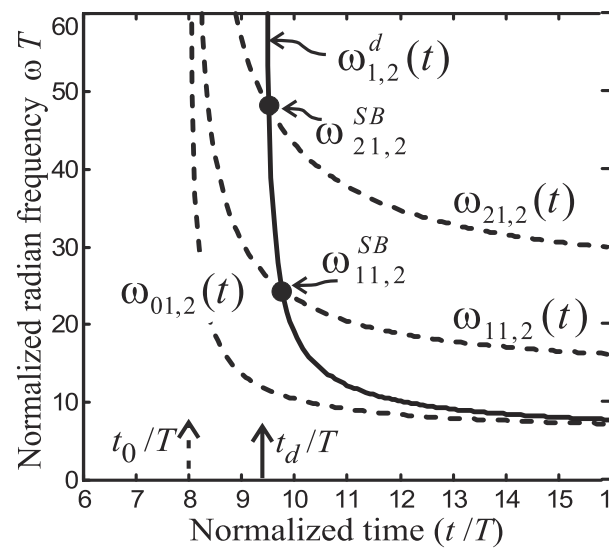

Figure 6. Normalized local instantaneous frequencies $T\omega_{pq,i}(t)$ and $T\omega^d_{q,i}(t)$ for FWs for and diffracted fields, respectively, with $i = 2$ (positive frequencies), $q = 1$ and $p = 0, 1, 2$, versus normalized time t/T, with $T = d_z/c$.

equality states that in the transition region, the dominant frequencies must satisfy $d\psi/d\omega = 0$, leading to $\omega_{pq,i}(t)$ in (18). This is not surprising since we have already encountered the same phenomenology in section 5.2 for $q = 0$ and $p \neq 0$; therefore, the asymptotic evaluation for an observer in the space-time-dependent pqth transition region can be carried out in a similar fashion. Here, however, we note that $d\delta_{pq}^2/d\omega = 2\delta_{pq}\cdot(d\delta_{pq}/d\omega) = 0$ for $\omega = \omega_{pq}^{SB}$ and thus from (41), $d\psi^d/d\omega = d\psi/d\omega$ for $\omega = \omega_{pq}^{SB}$. This demonstrates that if for a certain $t = t_{pq}^{SB}$, one has $\omega_{pq,i}(t_{pq}^{SB}) = \omega_{pq}^{SB}$, then also

$$\omega_{q,i}^{d}\left(t_{pq}^{SB}\right) = \omega_{pq,i}\left(t_{pq}^{SB}\right) = \omega_{pq}^{SB}. \tag{42}$$

In other words, the asymptotic evaluation carried out above for $\omega_{q,i}^{d}(t)$ substantially different from ω_{pq}^{SB} automatically patches onto the asymptotic evaluation in the transition region $\omega \approx \omega_{pq}^{SB}$, when the observer is located in space-time at the SB_{pq} (see section 5.2). Therefore the solution for $\hat{A}_q^d(\mathbf{r}, t)$ in (40) can be used for all ($\mathbf{r}$, t), inside and outside the transition regions.

[21] Behavior of local instantaneous frequencies: Space limitations prevent coverage of all possible combinations of phasing η_x and η_z, and FW indexes p, $q<0$. We only consider positive frequencies, i.e., those with $i = 2$. The behavior of negative frequencies ($i = 1$) is inferred by noting that $\omega_{pq,1}(\mathbf{r}, t) = -\omega_{-p,-q,2}(\mathbf{r}, t)$ and $\omega_{q,1}^{d}(\mathbf{r}, t) = -\omega_{-q,2}^{d}(\mathbf{r}, t)$ (see (18) and (38), respectively). Since $t_d \geq t_0$, the diffracted signal reaches the observer always later than (or simultaneously with, for $\phi = \phi_{00}$) the TD-FW signal, as is also confirmed observing the domain of the real instantaneous frequencies in Figure 6. There, the dynamics of both FW and diffracted field local instantaneous frequencies is compared for the simple but representative nonphased case $\eta_x = \eta_z = 0$. Width d_z used for normalization, the x-domain interelement spacing is $d_x = 0.1\ d_z$, the observer is placed at $\mathbf{r} \equiv (x, y, z) = (-0.05d_z, 8d_z, 0)$ and time and frequency are normalized through $T = d_z/c$. As predicted above, for certain $t = t_{pq}^{SB}$, one has $\omega_{q,i}^{d}(t^{SB}) = \omega_{pq,i}(t^{SB}) = \omega_{pq}^{SB}$, which means that at $t = t_{pq}^{SB}$ the pqth moving SB intercepts the stationary observer at $\mathbf{r}$. In that vicinity, the $\hat{A}_q^d$ behavior undergoes a dispersive transition that compensates for the truncation of the TD-FW_{pq}, and restores total field continuity at time $t = t_{pq}^{SB}$. Except for the moving SBs, the compensation mechanism in the TD is equal to that in the FD [see *Capolino et al.*, 2000c, section III-A], for $q \neq 0$.

6. Total "Observable" Field With Band-Limited Excitation

[22] We now construct the total field radiated by a planar semi-infinite array due to a physically realizable band-limited (BL) pulsed dipole excitation $\hat{G}(t)$ with spectrum $G(\omega)$. Accordingly, the factor multiplying $\delta(x' - nd_x)\delta(z' - md_z)$ in (2) becomes $G(\omega)\exp(-jk(\eta_x x' + \eta_z z'))$ for the FD dipole currents and $\hat{G}(t - (\eta_x x' + \eta_z z')/c)$ for the TD dipole currents. The total BL response $\hat{A}^{tot,BL}(\mathbf{r}, t)$ of the semi-infinite planar array is then obtained by (4) or by convolving the total TD impulse response with the BL signal, $\hat{A}^{tot,BL}(\mathbf{r}, t) = \hat{A}^{tot}(\mathbf{r}, t) \otimes \hat{G}(t)$, with $\otimes$ denoting the convolution $\hat{A} \otimes \hat{G} \equiv 1/(2\pi)\int_{-\infty}^{\infty}\hat{G}(t')\hat{A}(t - t')\,dt'$. The total field radiated by the semi-infinite array is thus represented as

$$\begin{aligned}\hat{A}^{tot,BL}(\mathbf{r}, t) &= \left\{\hat{A}_{00}^{FW,BL}U(\phi_{00} - \phi) + \hat{A}_{00}^{d,BL}\right\} \\ &+ \sum_{i=1}^{2}\left\{\sum_{p\neq 0}^{\infty}\hat{A}_{p0,i}^{FW,BL}U\left[\phi_{p0,i}(t) - \phi\right] + \hat{A}_{p0,i}^{d,BL}\right\} \\ &+ \sum_{i=1}^{2}\sum_{q\neq 0}\left\{\sum_{p=-\infty}^{\infty}\hat{A}_{pq,i}^{FW,BL}U\left[\phi_{pq,i}(t) - \phi\right] + \hat{A}_{q,i}^{d,BL}\right\},\end{aligned} \tag{43}$$

with terms in brackets pertaining to the results in sections 5.1, 5.2, and 5.3, respectively. In particular, $\hat{A}_{00}^{FW,BL}(\mathbf{r}, t) = \hat{G} \otimes \hat{A}_{00}^{FW}$ and $\hat{A}_{00}^{d,BL}(\mathbf{r}, t) = \hat{G} \otimes \hat{A}_{00}^{d}$ are obtained by numerical integration since they do not have a dominant frequency. All other terms with $p \neq 0$ and/or $q \neq 0$, in the second and third brackets in (43) have a dominant instantaneous frequency which allows the convolution to be replaced by sampling the excitation $G(\omega)$ in (4) at that frequency. In particular, $\hat{A}_{p0,i}^{FW,BL}(\mathbf{r}, t) = G[\omega_{p0,i}(t)]\hat{A}_{p0,i}^{FW}$ and $\hat{A}_{p0,i}^{d,BL}(\mathbf{r}, t) = G[\omega_{p0,i}(t)]\ \hat{A}_{p0,i}^{d}$ in the second bracket, while $\hat{A}_{pq,i}^{FW,BL}(\mathbf{r}, t) = G[\omega_{pq,i}(t)]\ \hat{A}_{pq,i}^{FW}$ and $\hat{A}_{q}^{d,BL}(\mathbf{r}, t) = G[\omega_{q,i}^{d}(t)]\hat{A}_{q,i}^{d}$ in the third bracket. As noted in section 5.2, the term $\hat{A}_{p0,i}^{d}$ has been evaluated using its dispersion relation inside the moving SB transition region, and therefore it is set equal to zero outside, where it is subdominant (see also *Capolino and Felsen* [2002, section VI] for an equivalent argument).

[23] We have so far avoided the "dilemma" posed by the presence of exponential phase factors (already observed and resolved by *Felsen and Capolino* [2000] and *Capolino and Felsen* [2002, 2003]) which render all (pq, i) TD wavefields in (43) complex. Guided by those earlier resolutions of the dilemma, we construct a real TD "observable" field by (+p, +q, 1), (−p, −q, 2) pairing. This is suggested by the symmetry property $\omega_{pq,1}(t) = -\omega_{-p,-q,2}(t)$ and $\omega_{q,1}^{d}(t) = -\omega_{-q,2}^{d}(t)$ for FW and diffracted field instantaneous frequencies, respectively (see (18) and (38)). While for FW one can follow the arguments of *Capolino and Felsen* [2003], for diffracted fields the situation is more involved since the argument of the Fresnel function F in (35) and (40) (inside $D(\omega)$) is negative for negative frequencies, i.e., for $i = 1$, and the

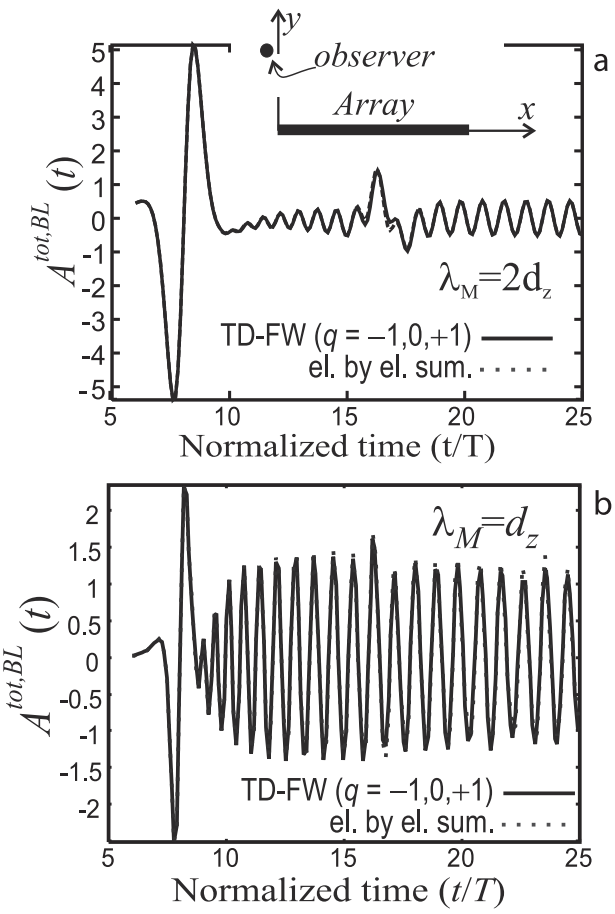

Figure 7. Radiated fields versus normalized time t/T, with $T = d_z/c$. The initial spikes are due to the $q = 0$ diffracted field from $x = 0$. The second spike in the edge-dominated response (a) is the $q = 0$ diffracted field arriving later from the edge at $x = 139d_x$; the chirped tail at the higher frequency in (b) is typical of a dispersive FW (here $q = -1, 1$).

property $F(-x) = F^*(x)$ for x real must be used. In particular, referring to the impulse-radiated field, one obtains $\hat{A}^{FW}_{p0,2} + \hat{A}^{FW}_{-p0,1} = 2\Re e\hat{A}^{FW}_{p0,2}$, $\hat{A}^{d}_{p0,2} + \hat{A}^{d}_{-p0,1} = 2\Re e\,\hat{A}^{d}_{p0,2}$, for the second bracket, and $\hat{A}^{FW}_{pq,2} + \hat{A}^{FW}_{-p,-q,1} = 2\Re e\hat{A}^{FW}_{pq,2}$, $\hat{A}^{d}_{q,2} + \hat{A}^{d}_{-q,1} = 2\Re e\hat{A}^{d}_{q,2}$, for the third bracket. Analogous relations hold for the BL field counterparts in (43), since $G(-\omega) = G^*(\omega)$, as required due to the real excitation $\hat{G}(t)$. Thus in (43) one should formally replace $\Sigma_{i=1}^{2}$ by $2\Re e$.

6.1. Numerical Examples

[24] Preliminary numerical experiments have been carried out for broad band, but band-limited, pulsed dipole excitation of a nonphased truncated dipole array in order to test the accuracy of the asymptotic solutions (43), and to compare the results with a reference solution obtained by element-by-element summation over the pulsed BL radiations from all dipoles, i.e., the (m, n) sum over the BL Green's functions $\hat{G}(t - R_{mn}/c)/(4\pi R_{mn})$, with $R_{mn} = ((x - nd_x)^2 + (z - md_z)^2 + y^2)^{1/2}$, $m, n = 0, \pm1, \pm2,\ldots$ The array is "infinite" along z but truncated along x at $x = 0$ and $x = 139\ d_x$. The (m, n)-series has been truncated at $|m|, |n| < 139$, which includes all nonnegligible element radiations along z. Interelement spacings are such that $d_z = 10\ d_x$ in order to highlight the new phenomena (with respect to the semi-infinite line array of *Capolino and Felsen* [2002]) due to the z-dispersion relation for diffracted fields (since $d_z \gg d_x$, all fields with $p \neq 0$ are negligible for the chosen BL excitation). Both $x = 0$ and $x = 139d_x$ truncation effects have been accounted for, treating the actual strip array as the difference between two semi-infinite arrays. BL excitation: normalized Rayleigh pulse $\hat{G}(t) = \Re e[j/(j + \omega_M t/4)^5]$ (i.e., $\hat{G}(0) = 1$); $G(\omega) = \pi(6\omega_M)^{-1}\ (j4\omega/\omega_M)^4\ \exp(-4|\omega|/\omega_M)$; central radian frequency $\omega_M = \pi c/d_z$ ($\lambda_M \equiv 2\pi c/\omega_M = 2d_z$) in Figure 7a, and $\omega_M = 2\pi c/d_z$ ($\lambda_M = d_z$) in Figure 7b. Observer location: $\mathbf{r} \equiv (x, y, z) = (-0.05d_z, 8d_z, 0)$ so that $\phi = 93.6°$; since $\phi_{0q} = 90°$, diffracted fields are in transition. Since $U(\phi_{0q} - \phi) = 0$, no FW_{0q} are present. Fields $\hat{A}^{tot,BL}(\mathbf{r}, t)$ in (43) are plotted versus normalized time t/T, with $T = d_z/c$. The near coincidence, at the observer, of the FW turn-on times $t_0/T = 8$ and the $(x = 0)$ edge-diffracted arrival $t_d/T = 8.02$ also implies that diffracted fields are in transition. The included asymptotic terms $p = 0$ and $|q| \leq 1$ (solid curve) adequately reproduce the reference solution (dotted curve), demonstrating good convergence of the TD-FW representation in both cases a) and b). To verify the compensation mechanism discussed in sections 5.1 and 5.3, a second numerical test has been performed with the observer at $\mathbf{r} \equiv (+0.05d_z, 8d_z, 0)$ slightly to the right of the SB_{0q} (now $\phi = 86.4°$), and therefore reached by the TD-FW_{0q}. The resulting fields agree with those in Figures 7a and 7b, thus confirming field continuity across the SB.

7. Conclusions

[25] The motivation and methodologies for the present study having been summarized in the abstract and introduction, we re-affirm that our basic approach to parameterizing and understanding periodicity-induced FW-based TD dispersion can be extended to successively more complicated planar array configurations. The results are again appealingly expressed in terms of periodicity-modulated TD GTD-like wave phenomena, nonuniform outside and uniformized inside transition regions, with novel interpretations of the truncation-induced edge diffractions. Work is in progress to refine

and extend the present preliminary asymptotic results beyond the parameter ranges included here, and to perform comprehensive numerical tests over broad parametric excursion, with emphasis on validation and error estimates. The outcomes will be submitted for separate publication. The final canonical problem to be addressed is the TD counterpart of the FD plane sectoral array of *Capolino et al.* [2000a] and *Maci et al.* [2001], which through inclusion of corner diffraction, lays the foundation for treating polygonal periodic planar array configurations.

[26] **Acknowledgments.** L.B. Felsen acknowledges partial support from ODDR and E under MURI grants ARO DAAG55-97-1-0013 and AFOSR F49620-96-1-0028, from the Engineering Research Centers Program of the National Science Foundation under award EEC9986821, from the US-Israel Binational Science Foundation, Jerusalem, Israel, under grant 9900448, and from Polytechnic University.

References

Capolino, F., and L. B. Felsen, Frequency and time domain Green's functions for a phased semi-infinite periodic line array of dipoles, *IEEE Trans. Antennas Propagat.*, *50*(1), 31–41, 2002.

Capolino, F., and L. B. Felsen, Time domain Green's functions for an infinite sequentially excited periodic planar array of dipoles, *IEEE Trans. Antennas Propagat.*, *51*(2), 2003.

Capolino, F., S. Maci, and L. B. Felsen, Asymptotic high-frequency Green's function for a planar phased sectoral array of dipoles, *Radio Sci.*, *35*(2), 579–593, 2000a.

Capolino, F., M. Albani, S. Maci, and L. B. Felsen, Frequency domain Green's function for a planar periodic semi-infinite dipole array: part I. Truncated Floquet wave formulation, *IEEE Trans. Antennas Propagat.*, *48*(1), 67–74, 2000b.

Capolino, F., M. Albani, S. Maci, and L. B. Felsen, Frequency domain Green's function for a planar periodic semi-infinite dipole array: part II. Phenomenology of diffracted waves, *IEEE Trans. Antennas Propagat.*, *48*(1), 75–85, 2000c.

Carin, L., and L. B. Felsen, Time harmonic and transient scattering by finite periodic flat strip arrays: Hybrid (ray)-(Floquet mode)-(MoM) algorithm, *IEEE Trans. Antennas Propagat.*, *41*(4), 412–421, 1993.

Felsen, L. B., and F. Capolino, Time domain Green's function for an infinite sequentially excited periodic line array of dipoles, *IEEE Trans. Antennas Propagat.*, *48*(6), 921–931, 2000.

Felsen, L. B., and L. Carin, Diffraction theory of frequency- and time-domain scattering by weakly aperiodic truncated thin-wire gratings, *J. Opt. Soc. Am. A*, *11*(4), 1291–1306, 1994.

Felsen, L. B., and N. Marcuvitz, Radiation and Scattering of Waves, Prentice Hall, Old Tappan, N. J., 1973.

Kouyoumjian, R. G., and P. H. Pathak, A uniform geometrical theory of diffraction for an edge in a perfectly conducting surface, *Proc. IEEE*, *62*(11), 1448–1461, 1974.

Maci, S., F. Capolino, and L. B. Felsen, Three dimensional Green's function for planar rectangular phased dipole arrays, *Wave Motion*, *34*(3), 263–279, 2001.

Rojas, R., Comparison between two asymptotic methods, *IEEE Trans. Antennas Propagat.*, *35*(12), 1489–1492, 1987.

F. Capolino, Department of Information Engineering, University of Siena, Via Roma 56, 53100 Siena, Italy. (capolino@ing.unisi.it)

L. B. Felsen, University Professor Emeritus, Polytechnic University, Brooklyn, NY 11201, USA. (lfelsen@bu.edu)